PNAS RESEARCH ARTICLE | MEDICAL SCIENCES

Sarcopenia phenotype and impaired muscle function in male mice with fast-twitch muscle-specific knockout of the androgen receptor

Tatsuya Hosoi[a], Mitsutaka Yakabe[a], Hiroko Sasakawa[a], Takayoshi Sasako[b], Kohjiro Ueki[c], Shigeaki Kato[d], Suzumi M. Tokuoka[e], Yoshiya Oda[e], Masahiro Abe[f], Toshio Matsumoto[g], Masahiro Akishita[a], and Sumito Ogawa[a,1]

Edited by Christopher Glass, University of California, San Diego, La Jolla, CA; received October 22, 2022; accepted December 19, 2022

Sarcopenia is distinct from normal muscle atrophy in that it is closely related to a shift in the muscle fiber type. Deficiency of the anabolic action of androgen on skeletal muscles is associated with sarcopenia; however, the function of the androgen receptor (AR) pathway in sarcopenia remains poorly understood. We generated a mouse model (fast-twitch muscle-specific AR knockout [fmARKO] mice) in which the AR was selectively deleted in the fast-twitch muscle fibers. In young male mice, the deletion caused no change in muscle mass, but it reduced muscle strength and fatigue resistance and induced a shift in the soleus muscles from fast-twitch fibers to slow-twitch fibers (14% increase, $P = 0.02$). After middle age, with the control mice, the male fmARKO mice showed much less muscle function, accompanied by lower hindlimb muscle mass; this phenotype was similar to the progression of sarcopenia. The bone mineral density of the femur was significantly reduced in the fmARKO mice, indicating possible osteosarcopenia. Microarray and gene ontology analyses revealed that in male fmARKO mice, there was downregulation of polyamine biosynthesis-related geneswhich was confirmed by liquid chromatography–tandem mass spectrometry assay and the primary cultured myofibers. None of the AR deletion-related phenotypes were observed in female fmARKO mice. Our findings showed that the AR pathway had essential muscle type- and sex-specific roles in the differentiation toward fast-twitch fibers and in the maintenance of muscle composition and function. The AR in fast-twitch muscles was the dominant regulator of muscle fiber-type composition and muscle function, including the muscle–bone relationship.

androgen | androgen receptor | fast-twitch muscle | polyamine | sarcopenia

Maintenance of the musculoskeletal system is essential for elderly individuals to lead an independent life. Sarcopenia is an age-related, progressive, and generalized skeletal muscle disorder that involves accelerated loss of muscle mass and function (1, 2). Although loss of muscle mass occurs in both slow-twitch (type I) and fast-twitch (type II) muscles, accelerated loss of motor units and fiber atrophy are seen primarily in fast-twitch muscle, and the proportion of total muscle cross-sectional area (CSA) occupied by type I fibers tends to increase in patients with sarcopenia (3, 4). These changes result in loss of mobility and increased risks of fall, fracture, physical disability, and frailty. It is important to elucidate the pathological mechanism of sarcopenia in order to prevent or ameliorate its debilitating effects on the growing elderly population.

Sarcopenia phenotypes have multifactorial causes beyond aging (2). We focused on the androgen–AR signaling pathway, which is expected to have strong and direct anabolic effects on skeletal muscle (5). With advancing age, men spend a significant proportion of their lives with declining serum levels of testosterone, which is the principal circulating androgen. Recent studies revealed the relationship between low serum testosterone levels and loss of muscle mass and strength (6, 7). Interventional studies showed that testosterone replacement therapy improved body composition and might be associated with modest increases in muscle strength (7); since then, there had been clinical interest in testosterone replacement as therapy for sarcopenia (8, 9). However, the mechanisms underlying the beneficial effect of testosterone replacement remain largely unresolved.

Androgens belong to the steroid hormone family and have an essential role in male sexual development and maintenance. They are mainly secreted from the testes, ovaries, and adrenal glands and have a variety of effects on target organs, including the prostate, muscles, bones, adipocyte tissues, and brain. The anabolic actions of androgens on skeletal muscle are predominantly mediated through the AR, which is the specific receptor for androgens. The AR is a ligand-dependent nuclear transcription factor that binds to DNA sequences called androgen response elements (AREs) and interacts with many coregulators to control the transcription of androgen target genes (10, 11). Androgen-signaling pathways are complex and involve both genomic and nongenomic mechanisms, including crosstalk with other signaling pathways (12).

Significance

The beneficial effects of the androgen–AR signaling pathway on sarcopenia have been pointed out, but the etiologic mechanism remains unsolved. Sarcopenia differs from usual muscle atrophy in that it is closely related to fiber-type shifts. This was one of our strong motivations to generate a new original mouse model of fast-twitch muscle-specific AR knockout in order to better understand the AR function in skeletal muscles. The model represented phenotypes of sarcopenia with aging and showed that the AR in fast-twitch muscles was the dominant regulator of muscle fiber-type composition and function. We also reported the importance of polyamine biosynthesis, which was regulated by AR, on muscle metabolism. These insights may pave the way for future drug development for sarcopenia.

Author contributions: T.H. and S.O. designed research; T.H., M.Y., and H.S. performed research; M.Y., H.S., T.S., K.U., S.K., S.M.T., Y.O., M. Abe, T.M., and S.O. contributed new reagents/analytic tools; T.H., M.Y., and S.O. analyzed data; S.K., T.M., and M. Abe provided intellectual input and critical review/comments; M. Akishita provided intellectual input and critical review/comments; and T.H., M. Akishita, and S.O. wrote the paper.

The authors declare no competing interest.

This article is a PNAS Direct Submission.

[1]To whom correspondence may be addressed. Email: suogawa@m.u-tokyo.ac.jp.

This article contains supporting information online at https://www.pnas.org/lookup/suppl/doi:10.1073/pnas.2218032120/-/DCSupplemental.

Published January 20, 2023.

In order to investigate the pathophysiologic roles of the AR in skeletal muscle in vivo, we generated a fast-twitch muscle-specific AR knockout (fmARKO) mouse model using Cre-loxP systems (13–16). MacLean et al. previously found that AR knockout (ARKO) caused decreased body mass and muscle mass and reduced force production by fast-twitch muscles in male mice but not in female mice (14). Subsequent studies using mice with myocyte-specific ARKO shed some light on the function of the AR in skeletal muscle, but they failed to distinguish the muscle fiber type-, sex-, or age-related AR function (15, 16).

Sarcopenia differs from normal muscle atrophy in that it is closely related to a shift in the muscle fiber type. By focusing on the fiber-type specificity of the AR function, we hoped to gain insight into the etiological basis of sarcopenia and, therefore, provide new avenues for therapeutic research. We generated a mouse model using Cre under the control of the myosin light chain 1f (Mlc1f) promoter to delete the AR, specifically in type II fast-twitch muscle fibers without affecting cardiac muscle (17, 18). Using that system, we clarified the muscle fiber-type-specific function of the AR and identified the genes and pathways related to the differentiation of fast-twitch and slow-twitch muscle fibers.

Results

fmARKO Was Validated in fmARKO Mice. To explore the AR function in skeletal muscle, we generated an fmARKO mouse strain by crossing two parental strains carrying Mlc1f-Cre and AR-flox, respectively (Fig. 1*A*). PCR analyses of tissues from male fmARKO mice confirmed the presence of the ARKO allele (600 bp fragment), specifically in skeletal muscle, which was quantitatively analyzed by ImageJ software (NIH) (Fig. 1*B*). The expression of AR messenger RNA (mRNA) in male fmARKO mice was fourfold lower in the soleus (SOL) muscle and 12-fold lower in the gastrocnemius (GAST) muscle, compared with that in the control mice, whereas there was no difference in AR mRNA expression in the cardiac muscle (Fig. 1*C*). Slow-twitch and fast-twitch fibers were present in roughly the same amount in the SOL muscles of both mouse strains, but fast-twitch fibers were more abundant than slow-twitch fibers in the GAST muscles; this might explain the lower rate of AR ablation in the SOL muscles of the fmARKO mice (19). Both mouse strains were capable of reproduction and grew normally with similar weight trends (Fig. 1*D*). fmARKO females also grew normally and the weight gain was similar in both mouse strains, although the average body weight was slightly but significantly greater in fmARKO mice than in control mice (*SI Appendix,* Fig. S1 *A* and *B*).

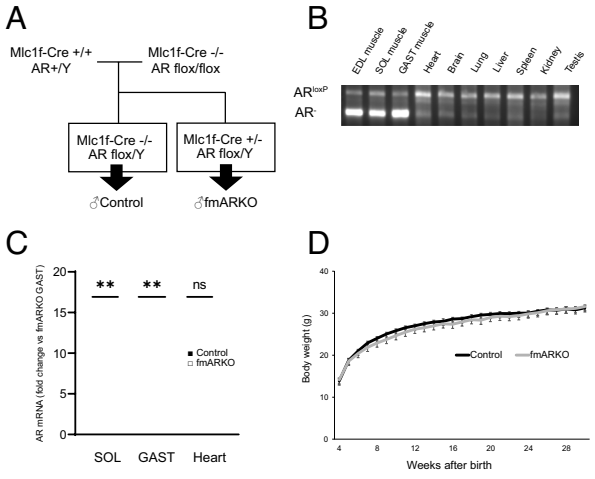

Fig. 1. Generation and characterization of fast muscle-specific androgen receptor knockout (fmARKO) mice. (*A*) Mlc1f-Cre+/+/AR-flox/Y mice were mated with AR-flox/flox mice to produce Mlc1f-Cre+/−/ARflox/Y mice (referred to as male fmARKO mice). (*B*) PCR analysis of tissue-specific recombination at the AR locus in different tissues from a 13-wk-old fmARKO mouse. The knockout allele (AR) is present only in skeletal muscle. (*C*) AR mRNA levels in skeletal and heart muscles of 13-wk-old control and fmARKO mice (n = 5 to 6/group). (*D*) Growth curves of control and fmARKO males (n = 6 to 13/group). Error bars indicate SEM; $^{**}P < 0.01$.

Muscle Strength Was Impaired Ahead of Muscle Mass in fmARKO Mice. Whole-body, hindlimb muscle, heart, and testes weights were examined in fmARKO and control mice. Compared with the control mice, the 13-wk-old fmARKO mice had no significant difference in the total body weight and hindlimb muscle/ heart weight, normalized by the total body weight. However, fmARKO male mice showed interesting changes as they aged and had lower hindlimb muscle mass after middle age (12 to 13 mo) (Table 1). The extensor digitorum longus (EDL) muscle mass was relatively unresponsive to androgens, and our fast-twitch muscle-specific AR ablation showed a neutral effect on EDL muscle mass (15, 16). To evaluate the effect of fast-twitch muscle-specific AR ablation on muscle function, a grip strength test, wire hang test, and treadmill running experiment were set up. With aging, the muscle function decreased progressively in all tests (Fig. 2*A*). Compared with control mice, 13-wk-old fmARKO mice showed less muscle strength and endurance capacity, based on the 10% decline in grip strength (g/g) and 32% decline in total work output (J) ($P = 0.02$, $P = 0.03$, respectively). The maximum time to fall in the wire hang test was over 120 s in all 13-wk-old mice, and no significant difference in the holding impulse (Ns) was observed (Fig. 2*B*). Compared with control mice, fmARKO mice at 12 to 13 mo of age showed 33% lower grip strength ($P < 0.001$), 74% lower holding impulse ($P = 0.03$), and 64% lower total work output ($P = 0.01$) (Fig. 2*C*). In addition, less muscle function was observed in 2-y-old fmARKO mice, although the muscle function in aged mice was sufficiently impaired regardless of AR ablation, and the difference became smaller (Fig. 2*D*). Moreover, although these physical performance assessments were informative, the results might have been confounded by systemic changes. Therefore, we also set up an ex vivo functional assessment of muscle in insolation and measured the maximal muscle contraction force (g) of the GAST muscle using sciatic nerve stimulation. In 12- to 13-mo-old mice, muscle contraction was significantly lower in fmARKO mice than in control mice ($P < 0.01$) (Fig. 2*E*).

We also focused on the AR function in females and examined fmARKO female mice, in comparison with control female littermates; however, differences in muscle-related phenotypes were not observed (*SI Appendix,* Table S1 and Fig. S1*C*). Taken together, our results indicated that male fmARKO male mice had decreased muscle strength and lower endurance capacity despite the maintenance of normal hindlimb muscle mass at a young age, suggesting that the AR function might have affected muscle quality. Moreover, impaired muscle mass was observed in male fmARKO mice after middle age, suggesting that muscle strength was impaired ahead of muscle mass.

Muscle–Bone Interaction Was Implied in the fmARKO Mice. The fmARKO mice at 13 wk of age demonstrated an increase in testicular mass by 11% ($P < 0.001$), although the difference reversed as they aged (Table 1). We focused on the interaction between the reproductive system and bone because the bone was reported to be an endocrine regulator of reproduction through osteocalcin (OCN), which is an osteoblast-specific secreted molecule (20). Moreover, there is a crosstalk between sarcopenia and osteoporosis (i.e., osteosarcopenia), and low muscle strength has been associated with a more rapid decline in bone mineral density (BMD) (1, 21). In this study, we confirmed the presence of impaired muscle strength in fmARKO mice starting at 13 wk of age; therefore, we assumed a relatively low BMD in this group.

The overall serum testosterone level was not different between male fmARKO mice and control mice (Fig. 3*A*). Similarly, the serum OCN and tartrate-resistant acid phosphatase (TRAP) levels were not different, suggesting that

Table 1. Total body weight and hind limb muscle, heart, and testis mass (mg) normalized by body weight (g) in male mice

	13 wk		12 to 13 mo		2 y	
	Control (n = 12)	fmARKO (n = 11)	Control (n = 4)	fmARKO (n = 3)	Control (n = 7)	fmARKO (n = 3)
Total body weight (g)	25.2 ± 0.7	24.3 ± 0.6	28.6 ± 1.1	32.2 ± 1.8	32.2 ± 0.4	32.4 ± 2.1
Gastocnemius (mg/g)	5.7 ± 0.1	5.8 ± 0.1	5.3 ± 0.1	4.5 ± 0.2**	4.3 ± 0.1	3.7 ± 0.2**
Soleus (mg/g)	0.35 ± 0.01	0.32 ± 0.01	0.30 ± 0.01	0.26 ± 0.01*	0.26 ± 0.01	0.15 ± 0.03***
EDL (mg/g)	0.46 ± 0.03	0.44 ± 0.02	0.37 ± 0.02	0.32 ± 0.02	0.33 ± 0.02	0.26 ± 0.05
Tibialis (mg/g)	2.4 ± 0.1	2.3 ± 0.1	2.2 ± 0.1	1.8 ± 0.1**	1.8 ± 0.1	1.5 ± 0.1*
Hearts (mg/g)	5.8 ± 0.2	5.6 ± 0.1	5.9 ± 0.5	5.7 ± 0.2	5.1 ± 0.2	5.5 ± 0.5
Testis (mg/g)	3.7 ± 0.1	4.1 ± 0.1***	3.6 ± 0.2	3.0 ± 0.1**	2.9 ± 0.1	2.7 ± 0.1

Data are expressed ± SE.
*P < 0.05, **P < 0.01, ***P < 0.001, fmARKO compared with control mice.
EDL, extensor digitorum longus.

deletion of the AR in muscles did not influence bone function as an endocrine regulator of reproduction (Fig. 3*B*). On the other hand, BMD in male fmARKO mice was significantly decreased in both trabecular and cortical bone, compared with that in control mice (P = 0.01 and P = 0.04, respectively; Fig. 3 *C* and *D*), indicating the possibility of osteosarcopenia. Those phenotypes were not observed in female fmARKO mice (Fig. 3 *E* and *F*). The reasons for these discrepancies were unknown, and further studies, such as bone morphometry analysis, are needed.

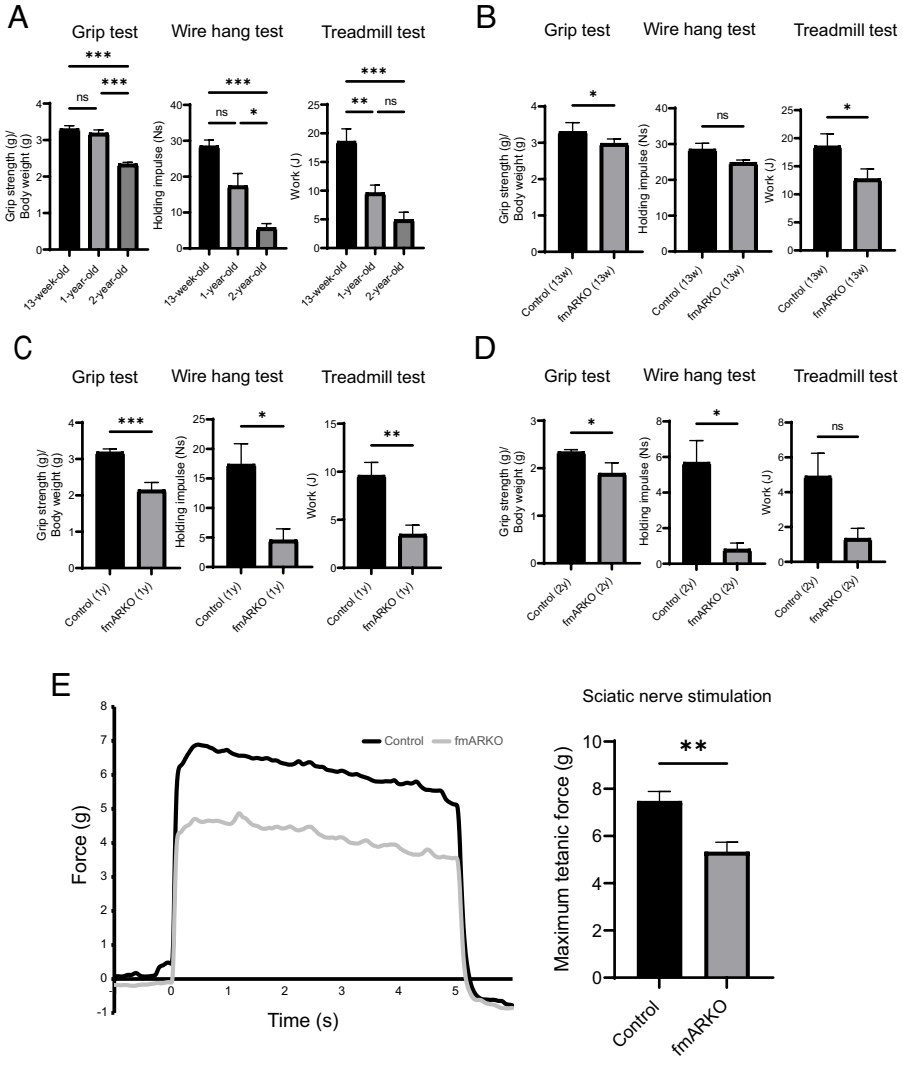

Fig. 2. fmARKO mice showed lower muscle strength and endurance capacity. (*A*) The results of grip test [forelimb maximal grip strength normalized for body weight (g/g)], wire hang test [holding impulse (Ns)], and treadmill test [total work output (J)] in 13-wk-old, 12- to 13-mo-old, and 2-y-old control mice (n = 3 to 8/group). (*B*–*D*) The results of grip test, wire hang test, and treadmill test were compared between control and fmARKO mice at (*B*) 13-wk-old, (*C*) 12- to 13-mo-old, and (*D*) 2-y-old (n = 3 to 8/group). (*E*) In situ GAST muscle tetanic contraction during sciatic nerve stimulation and the maximal muscle contraction force (n = 3 to 7/group). Error bars indicate SEM; *P < 0.05, **P < 0.01, ***P < 0.001.

The Proportion of Slow-Twitch Fibers Was Increased in the Skeletal Muscles of Male fmARKO Mice. Hematoxylin and eosin (H&E) and nicotinamideadenine dinucleotide dehydrogenase-tetrazolium reductase (NADH-TR) staining of the SOL specimens showed little morphological difference between the 13-wk-old control and fmARKO mice; however, Oil Red O staining revealed lipid droplets in the muscle fibers of the male fmARKO mice but not in those of the control mice, indicating a difference in lipid metabolism (Fig. 4*A*). Examination of the blood levels of total cholesterol (TC), triglycerides (TG), low-density lipoprotein cholesterol (LDL-C), high-density lipoprotein cholesterol (HDL-C), and adiponectin showed no differences between fmARKO and control mice. This result suggested that the difference in lipid metabolism was limited in muscle tissue (*SI Appendix,* Fig. S2*A*). In addition, we confirmed that the adiponectin level was significantly higher in female mice than in male mice ($P < 0.01$), as previously reported (22).

In mice, skeletal muscle fibers are classified into four different types (i.e., I, IIa, IIx, and IIb). The slow type I fibers are aerobic and suited

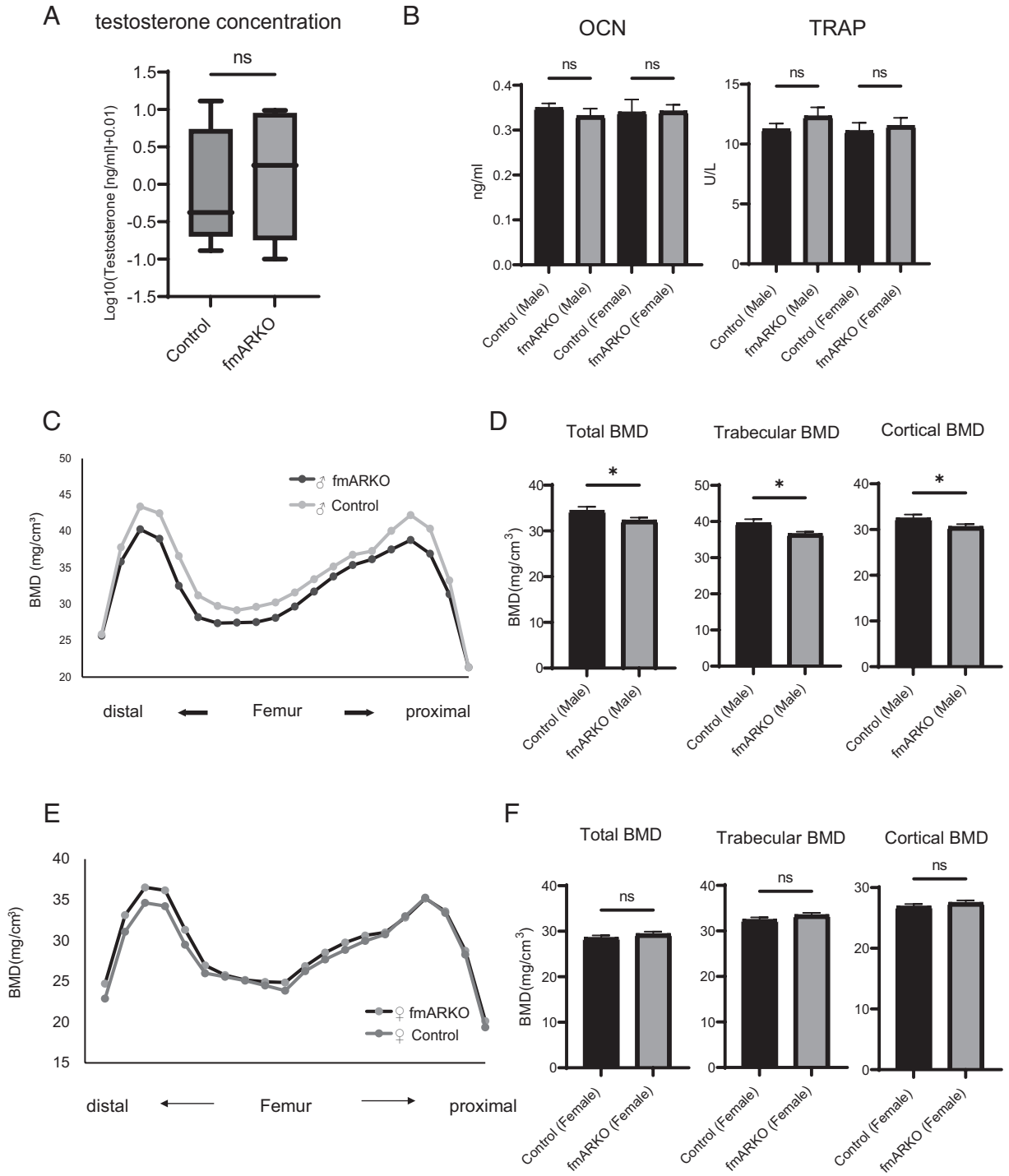

Fig. 3. Muscle–bone interaction was indicated in the fmARKO mice. (*A*) Serum levels of testosterone presented as log10 (x + 0.01) values. The highest and lowest values and the interquartile range from the first quartile to the third quartile are shown (n = 8/group). (*B*) Serum levels of OCN and TRAP (n = 5 to 13/group). (*C* and *D*) Total (n = 3, 60 points/group), trabecular (24 points), and cortical (30 points) BMD were evaluated, and bone loss in the whole femurs of 13-wk-old male fmARKO mice was shown. (*E* and *F*) Total (n = 3, 60 points/group), trabecular (24 points), and cortical (30 points) BMD were evaluated, and there were no differences between the female fmARKO mice and controls. Error bars indicate SEM; *$P < 0.05$.

for prolonged low-power work, whereas the fast-type IIx and IIb fibers are anaerobic and adapted for brief and intense contractions. The type IIa fibers are intermediate between the slow and fast fibers but are most similar to the type I fibers. To investigate the function of the AR in the regulation of muscle fiber type, we used immunostaining of the SOL muscles to examine the fiber-type distribution. The staining for the slow-twitch and fast-twitch myofiber markers compensated each other, and the SOL muscles of 13-wk-old mice were full of muscle fibers without atrophy. This enabled us to focus on the results from the fast-twitch myofiber marker myosin heavy chain (MHC) type 2. The percentage of slow-twitch fibers was increased by 14% in male fmARKO mice, compared with that in control mice ($P = 0.02$; Fig. 4*B*), which is similar to what is often observed in patients with sarcopenia. The mean CSA of slow-twitch fibers and fast-twitch fibers tended to be lower in the fmARKO mice than in the control mice, without reaching statistical significance (Fig. 4*C*). In female fmARKO mice, there were no significant differences in comparison with control mice (*SI Appendix,* Fig. S2 *B–D*).

Expression of Genes Related to Muscle Fiber Type and Muscle Mass Was Altered in fmARKO Mice. To explore the cause of the differences in muscle fiber composition, we examined the mRNA levels of the genes related to muscle fiber type in 13-wk-old mice. Myoglobin, slow troponin I (TnI slow), sarcomeric mitochondrial creatine kinase (sMtCK), and MHC type I are expressed primarily in slow fibers, whereas parvalbumin, muscle creatine kinase (MCK), MHC type IIA, and MHC type IIB are expressed predominantly in fast fibers (23). TnI slow and MHC type I showed a 3.3- ($P = 0.01$) and 4.6-fold ($P < 0.01$) increase in expression, respectively, compared with those in control mice. On the other hand, the expression levels of fast fiber-related genes were not changed by the AR ablation (Fig. 4*D*). MyoD, which belongs to the myogenic regulatory factor family of transcription factors, is preferentially expressed in fast-twitch muscles, and is related to muscle fiber-type plasticity (4). Inhibition of MyoD activates slow fiber-related genes and leads to the transformation of type II fibers to type I fibers (24, 25). In fmARKO mice, the mRNA level of MyoD decreased by 2.6-fold, compared with that in control mice ($P = 0.02$; Fig. 4*E*). Taken together, the results demonstrated that fast-twitch muscle-specific AR ablation caused a shift in muscle fiber type by inhibiting MyoD expression and, therefore, increasing the expression of slow fiber-specific genes.

In line with findings in other ARKO mouse models, the mRNA level of myostatin, which is a member of the transforming growth factor-β protein family, decreased by 2.3-fold in fmARKO mice, compared with that in control mice ($P < 0.01$; Fig. 4*E*) (14, 26). Myostatin inhibits muscle growth, and its gene expression is regulated by androgens (26). Therefore, its downregulation in fmARKO mice might have contributed to the maintenance of muscle mass, CSA, and muscle fiber diameter.

The muscle-specific E3 ubiquitin ligases Muscle RING finger 1 (MuRF1) and muscle atrophy F-box protein-1 (MAFbx)/Atrogin-1 are normally expressed in skeletal and heart muscles and are upregulated in atrophying muscles. In fmARKO mice, the mRNA levels of MuRF1 and MAFbx/Atrogin-1 were decreased, compared with those in control mice ($P = 0.03$ and $P = 0.03$, respectively), which might have contributed to the preservation of muscle mass after AR ablation (Fig. 4*E*). Although MAFbx/Atrogin-1 was reported to interact with the MyoD for its degradation (27, 28), there was no change in MyoD protein, probably because of the suppressed MyoD mRNA level (*SI Appendix,* Fig. S4*C*). In contrast to the results in male mice, no changes in gene expression following ARKO were observed in female mice (*SI Appendix,* Fig. S3 *A* and *B*).

Shift in Muscle Fiber Type in fmARKO Mice Was Independent of the Calcineurin A/ Nuclear Factor of Activated T Cells Cytoplasmic 1 (NFATc1) Pathway in the Translational Level. Calcineurin signaling is one of the major pathways in muscle fiber-type plasticity related to MyoD. Calcineurin A (CnA) is a calcium-regulated serine/ threonine phosphatase that was previously reported to be repressed by the AR and to play a major role in mediating muscle fiber type (4, 14, 29). Moreover, the mRNA level of CnA was found to increase in mice with whole-body ARKO and in orchiectomized male mice (14). CnA dephosphorylates and activates the NFATc1 transcription factor, which in turn activates the expression of slow muscle-specific genes and inhibits MyoD activity (4, 24, 30). A transgenic mouse model, in which CnA was activated in skeletal muscle, showed an increase in slow muscle fibers with no change in skeletal muscle mass (24); this was similar to the phenotype observed in the 13-wk-old male fmARKO mice. Contrary to our expectations, however, the mRNA and protein levels of CnA/NFATc1 were not different between male fmARKO mice and control mice (*SI Appendix,* Fig. S4 *A* and *B*). Although NFAT activation is also regulated by posttranslational modification, these results indicated that the shift in fiber type observed in fmARKO mice was independent of the CnA/ NFAT pathway in the translational level.

Polyamine-Related Gene Expression Was Altered in Male fmARKO Mice. AR is a ligand-inducible transcription factor with many target genes. We performed microarray and quantitative real-time PCR (qPCR) experiments to identify the AR target genes that accounted for the structural and functional differences between the muscles of male fmARKO mice and control mice. A suite of 195 genes showed twofold or greater differences in the expression of genes ($P < 0.05$ for each), including 151 genes that were downregulated and 44 genes that were upregulated in the fmARKO mice, compared with the findings in the control mice (Fig. 5 *A* and *B*). A gene ontology (GO) enrichment analysis showed significant changes in the expression levels of polyamine biosynthesis-related genes, including genes related to the polyamine and spermine (SPM) metabolic processes (Fig. 5*C* and Dataset S1). The mRNA expression levels of S-adenosylmethionine decarboxylase (Amd1, 2), ornithine decarboxylase (Odc1), and spermine oxidase (Smox) were 8.0-fold to 17.6-fold significantly lower in male fmARKO mice than in control mice (Fig. 5*D*). These results were partially supported by previous studies (16, 31, 32). Like the genes related to muscle type, the polyamine biosynthesis-related genes showed no changes in expression in female fmARKO mice, in comparison with control mice (*SI Appendix,* Fig. S3*C*).

The principal examples of polyamines are putrescine (PUT), spermidine (SPD), and SPM, which are maintained at optimum concentrations. In 13-wk-old mice, we examined the polyamine levels in the GAST muscle using LC-MS assay and found that SPM was significantly decreased in fmARKO mice than in control mice, but there were no differences in PUT and SPD (Fig. 5*E*). We also assessed polyamine metabolism and polyamine levels in vitro using primary myoblast cultures. In myoblasts derived from the control mice, polyamines were present, albeit scarce, and increased in concentration in response to 24 h of 5α-dihydrotestosterone (DHT) treatment (Fig. 5*F*). On the other hand, myoblasts derived from male fmARKO mice showed no signs of polyamines prior to DHT but had detectable polyamine levels after DHT treatment. Decreased levels of polyamines were previously observed in the skeletal muscles of aged mice, and a strong association between polyamine levels and skeletal muscle mass has been demonstrated (32–34). Our results revealed impaired polyamine metabolism in male fmARKO skeletal muscle and the possibility of its restoration after DHT treatment; this indicated a strong association between androgens, polyamines, and sarcopenia.

There Was No Difference in Autophagy between fmARKO Mice and Control Mice. Polyamines, especially SPD, are the inducers of autophagy and promote longevity in an autophagy-dependent manner (35, 36). Autophagy is a cellular process to maintain homeostasis through self-digestion of unnecessary or dysfunctional components via autophagosomes. Autophagy is also thought to play a pivotal role in muscle maintenance (37, 38). We measured the mRNA levels of the autophagy-related genes *Atg2A*, *5*, *7*, *9A*, *12*, and *14*; *autophagy-adaptor protein p62*; *WD-repeat protein*

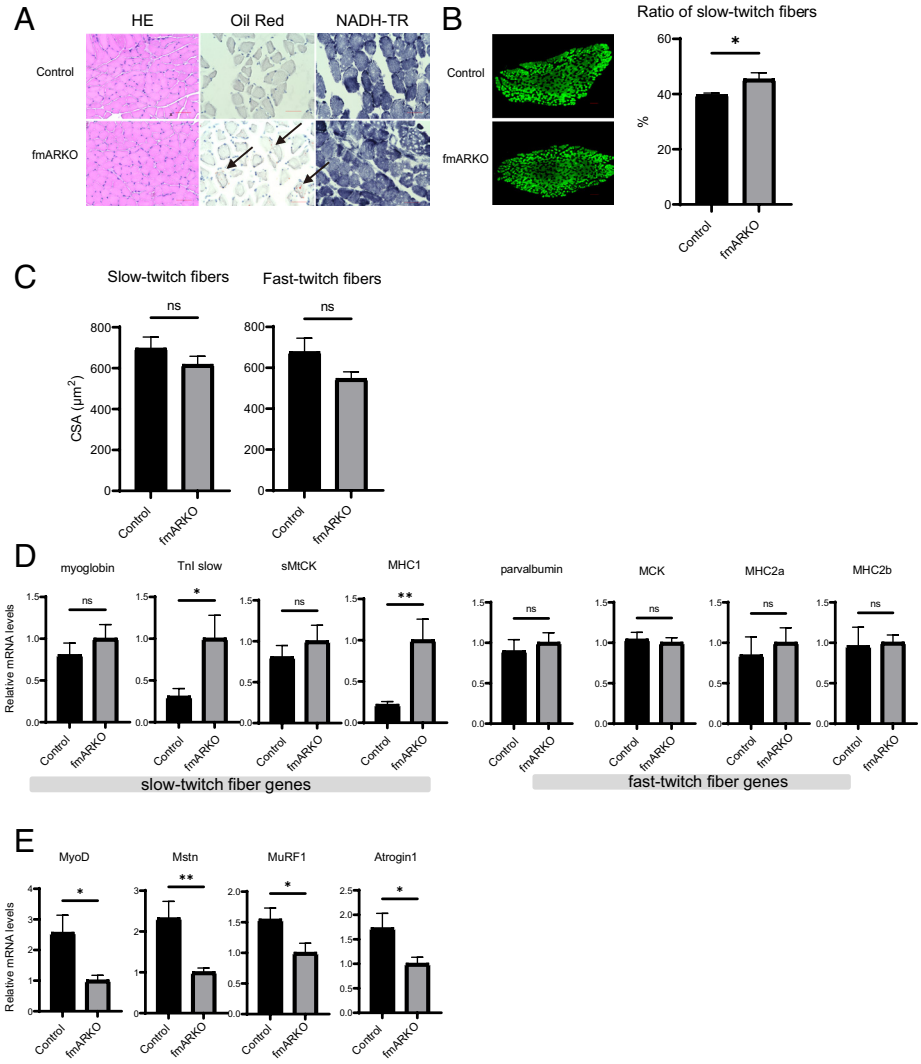

Fig. 4. Fast muscle-specific androgen receptor ablation increased the proportion of type I fibers in SOL muscle and altered expression of genes related to muscle fiber type. (*A*) Histological analysis of H&E, Oil Red O, and NADH-TR staining of SOL muscles from male 13-wk-old control and fmARKO mice. (Scale bar, 50 μm.) Black arrowheads indicate lipid droplets inside the muscle fibers of fmARKO mice. (*B*) Representative images of immunohistochemically stained SOL muscle from control and fmARKO mice. Fast-twitch fibers are stained green; slow-twitch fibers are blacked out. (Scale bar, 100 μm.) The mean ratios of slow-twitch fibers are shown (n = 5/group). (*C*) Mean fiber CSA of slow-twitch and fast-twitch fibers (n = 5/group). (*D* and *E*) Real-time PCR was used to measure gene expression of fiber-specific transcripts and muscle mass-related transcripts (n = 7 to 8/group). Error bars indicate SEM; $*P < 0.05$, $**P < 0.01$.

interacting with phosphoinositide 2 (*WIPI2*); *Unc-51-like kinase 1* (*ULK1*); and the *focal adhesion kinase family-interacting protein of 200 kD* (*FIP200*). The expression levels of these genes tended to decrease by 1.1-fold to 2.9-fold in male fmARKO mice, compared with those in control mice, although none of the changes were statistically significant (*SI Appendix,* Fig. S5*A*). Loss of autophagy function was previously reported to induce p62 accumulation, but we found no difference in the p62 protein levels between the control mice and fmARKO male mice (*SI Appendix,* Fig. S5*B*). H&E staining of the SOL and GAST muscles showed no change in the myofiber size and no features of degeneration, including macrophage infiltration, foci of inflammation, and necrotic fibers. Therefore, our mouse model showed no significant changes in autophagy in relation to ARKO.

Discussion

As we age, we experience sarcopenia, which is loss of muscle mass and strength. Sarcopenia has multiple causes, but one of the main causes is thought to be age-related changes in anabolic hormone levels. Androgen deficiency was reported to influence muscle mass and cause sarcopenia, partly by altering protein balance and can be ameliorated by androgen replacement therapy (2, 7). In patients with sarcopenia, fast-twitch muscle fibers, compared with slow-twitch muscles, are typically more prone to atrophy and loss of function. Therefore, we might expect a causal relationship between androgens and muscle fiber type, although the underlying molecular mechanisms remain poorly understood.

Although the androgen-signaling pathways are complex, most of the effects of androgens occur through binding to the AR (12). Muscle-specific ARKO mice models using the MCK promoter (MCK-Cre) and the α-skeletal actin promoter (α-skeletal actin (HSA)-Cre) have been developed to study the AR function in muscles, and they showed different results (15, 16). Mice with both types of ARKO showed little change in skeletal muscle mass. Mice with the MCK-Cre knockout showed no change in muscle strength or fatigue, whereas those with the HSA-Cre knockout showed decreased muscle strength. In the SOL muscles of mice with the MCK-Cre knockout, AR ablation was accompanied by conversion of fast fibers to slow fibers, indicating that the myocytic AR functioned to regulate the muscle fiber types. In addition, conversion of fast fibers to slow fibers in the SOL muscles along with decreased

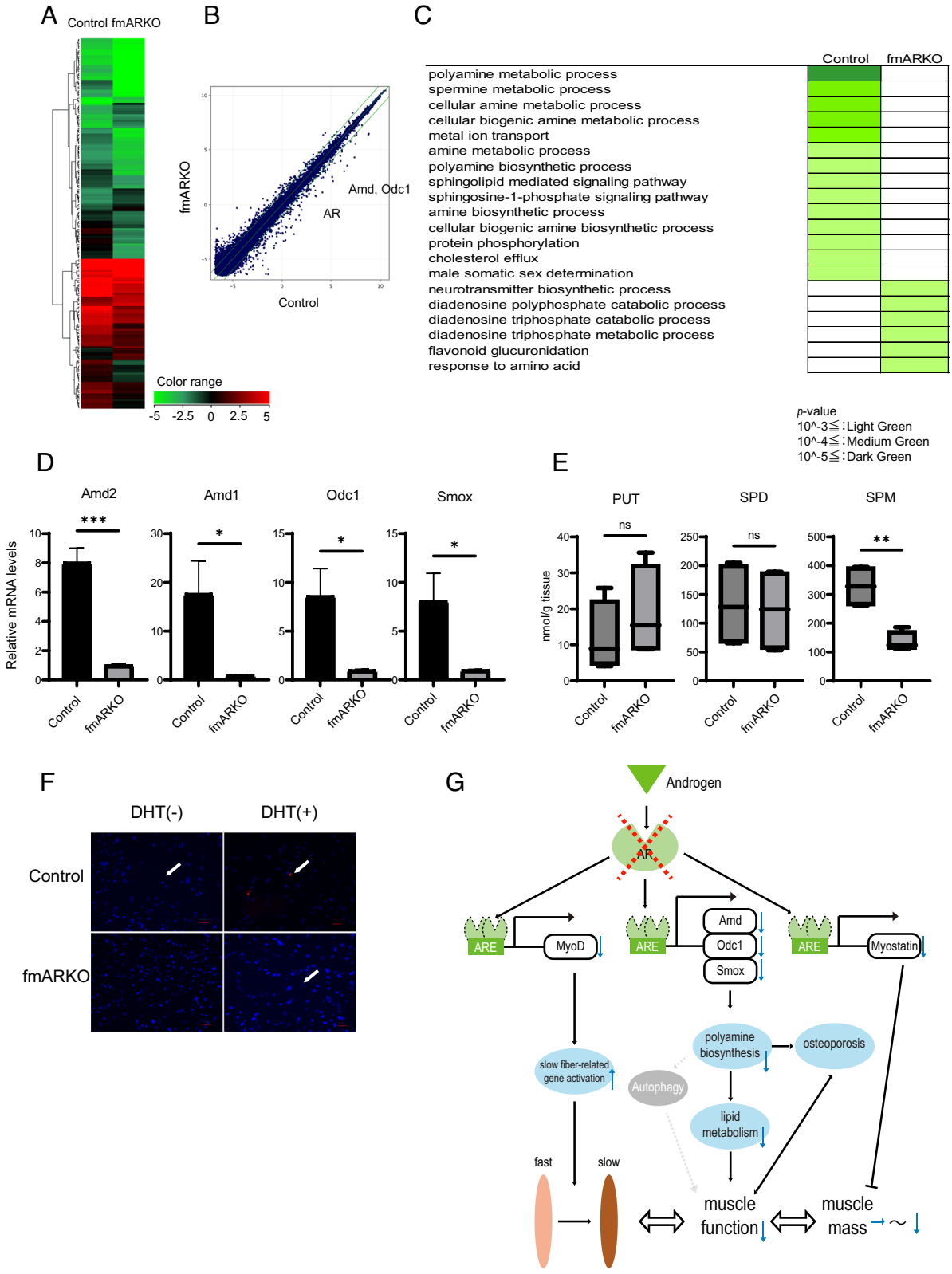

Fig. 5. Polyamine-related gene expression was highly altered in male fmARKO mice. (*A*) A heatmap shows genes that were significantly upregulated or downregulated in male fmARKO mice in comparison with control mice. (*B*) A scatter plot illustrates responses of genes with at least a twofold increase in expression in fmARKO mice in comparison with control mice. (*C*) Representative functional annotations corresponding to biological process terms in a GO enrichment analysis. Expression levels of polyamine biosynthesis-related genes were significantly altered after ARKO. Color coding corresponds to the following *P* values; ≤10^{-3} light green; ≤10^{-4} medium green; ≤10^{-5} sdark green. (*D*) Real-time PCR showed the gene expression of polyamine biosynthesis-related transcripts (n = 7 to 8/group). (*E*) LC-MS assay showed that SPM was significantly decreased in fmARKO mice compared with control mice (n = 4/group). (*F*) Primary culture of myoblasts derived from control and fmARKO mice. PolyamineRED detection of polyamine revealed no sign of polyamines in untreated fmARKO mice, although they were detected after DHT treatment (white arrowheads). (*G*) Schematic model of androgen–androgen receptor signaling in skeletal muscle of male fmARKO mice. Androgen enters the cell and binds to the androgen receptor. The androgen receptor then binds to androgen response elements in DNA to control the transcription of target genes such as MyoD, Odc1, and Myostatin. The target genes interact with each other and regulate the distribution of muscle fiber type, muscle function, and muscle mass. The activation of target pathways varies according to sex and the surrounding environment. Error bars indicate SEM; *$P < 0.05$, **$P < 0.01$, ***$P < 0.001$.

grip strength was shown in satellite cell-specific ARKO (26). Previous studies provided insights into the role of the AR in skeletal muscle. However, their results were inconsistent; did not focus on the fiber type-, sex-, or age-related roles of the AR function; or did not exclude the impact of AR ablation on cardiac muscles. We used Cre under the control of an Mlc1f promoter in order to generate a fast-twitch specific ARKO model; this is a well-designed model with high selectivity so that we could advance the pathophysiological studies of sarcopenia, characterized by fast-twitch dominant atrophy (39). This model further enables us to examine the AR regulation in fast-twitch muscles, compare the AR function in fast- and slow-twitch muscles, and reveal the crosstalk between fast- and slow-twitch muscles together with the muscle–bone relationship.

Analyzing this model, we found that the AR regulated multiple pathways in skeletal muscles and bone. The fast-twitch muscle-specific deletion of the AR in male mice significantly affected muscle function, fiber type, metabolism, and muscle–bone relationship by regulating the transcription of androgen target genes (Fig. 5*G*). In agreement with previous results, our results showed no differences in the hindlimb muscle mass and the CSA of muscle fibers between 13-wk-old male fmARKO mice and control mice, supporting the hypothesis that the AR in muscle does not control postnatal growth or there were compensatory mechanisms (16). AR deletion in fast-twitch muscle reduced muscle strength and fatigue resistance and caused a shift from fast-twitch to slow-twitch fibers. Although AR deletion was limited to fast-twitch muscles in the fmARKO mice, the proportion of slow-twitch fibers in the SOL muscles of these mice increased by 14%, along with a proportional decrease in fast-twitch fibers. These results, in comparison with the results of previous studies on muscle-specific ARKO mice (i.e., 10% more type I fibers in SOL muscles), indicated that the AR in fast-twitch muscle, rather than that in slow-twitch muscle, was the dominant regulator of fiber-type composition (15). Interestingly, fmARKO mice had lower hindlimb muscle mass after middle age, suggesting a change in the role of the AR over time. Muscle strength was impaired ahead of muscle mass in fmARKO mice, similar to the progression of sarcopenia, suggesting that sarcopenia might originate in fast-twitch muscle.

Shifts in muscle fiber type between fast and slow varieties occur in some muscle diseases and interventions. In many cases, MyoD activity plays a central role in regulating muscle fiber-type differentiation and plasticity (4, 40, 41). MyoD is assumed to be one of the androgen target genes, and treatment of C2C12 myoblasts with an AR agonist was reported to increase the messenger RNA (mRNA) levels of MyoD (12, 42). Compared with control mice, male fmARKO mice were found to have decreased mRNA level of MyoD and increased number of slow fiber-related genes. An association between the muscle fiber-type shift and the CnA/ NFAT pathway, which was another major candidate for governing differential gene expression, was not shown in male fmARKO mice (40). Taken together, our results indicated that deletion of the AR directly downregulated MyoD expression, leading to the upregulation of slow fiber-related genes and a shift in the fiber type in skeletal muscles. Whether this difference in fiber-type composition was secondary to myogenesis from undifferentiated myoblasts to differentiated fibers (differentiation), fiber-type conversion (trans-differentiation), or other processes is a subject for future analysis.

The association between the AR and polyamine was also a key conclusion in this study. The loss of polyamines per se might be a factor in sarcopenia or osteoporosis, as suggested by the observed loss of polyamines in the muscles of older mice (33, 36, 43). Some key enzymes that control polyamine biosynthesis contain AREs, and this study confirmed that polyamine biosynthesis was regulated by the AR signaling pathway (29). Moreover, as shown in the GO analysis, among the polyamine biosynthesis processes, the SPM metabolic process was especially downregulated; this was supported by the liquid chromatography-mass spectrometry (LC-MS) assay. SPM was reported to be more effective than PUT or SPD in higher mammals, and our results indicated that it played an important role in this new mouse model (44). Skeletal muscle mitochondria are essential for muscle viability and function, and the functional linkage between polyamine and mitochondrial metabolism is recently reported (45). This linkage might be the potential mechanisms of the sarcopenia phenotype observed in this study. The functional linkage between polyamine and fatty acid metabolism is also known (46), and our histological analysis of skeletal muscles with Oil Red O staining suggested a certain change in lipid metabolism. A combination of these changes in metabolism might result in poor muscle quality. Japanese and Mediterranean diets, which are known as macrobiotic diets, are abundant in polyamines. Oral intake of these polyamine-rich diets was reported to increase the blood SPM levels in both mice and humans and resulted in multifaceted benefits on survival (47, 48). Therefore, this study pointed out the possibility of SPM as a future therapeutic agent for age-related pathologies, including sarcopenia. Moreover, polyamine was suggested to be one of the autophagy inducers, and low polyamine levels led to restrained autophagy (35). Previous studies showed that autophagy preserved muscle mass and function through muscle metabolic balance, demonstrating a close relationship between autophagy and sarcopenia (37, 38, 49). In this study, after AR deletion, we found no changes in the GO analysis and in the mRNA levels of autophagy-related genes, p62 protein levels, or myopathic phenotypes in the morphological analyses. However, our study on the polyamine–autophagy axis was limited, and further investigation, such as the use of electron micrographs, is worth pursuing.

In summary, we generated a sarcopenia mouse model with fast-twitch muscle-specific AR ablation; we found this model to be a valuable in vivo model to study the AR function in a muscle type-specific manner. Our results indicated that the AR in fast-twitch muscles, rather than in slow-twitch muscles, was the dominant regulator of muscle fiber-type composition and function and that biosynthesis of polyamines played an important role in muscle function. In addition, we found that androgens played little or no role in determining muscle mass, muscle function, or musculoskeletal linkage in females. Although the cause of the differences in the AR function between muscle types and sex remained unclear, our results suggested that selective AR modulators, especially those affecting fiber-type-specific AR functions, or polyamines, especially SPM, might be used as therapeutic agents for sarcopenia, with fewer side effects, compared with current treatments. Further studies, such as examining transgenic mice with muscle-specific over-expression of AR, directly comparing the functional differences among muscle-specific ARKO, slow-twitch-specific ARKO, and fmARKO mice, or deleting AR function specifically in adult mice employing a tamoxifen-inducible Cre-loxP strategy, would provide more insights into the muscle fiber-type-specific roles of the AR.

Materials and Methods

Mice. We generated fmARKO mice using the Cre-loxP strategy. AR-flox/flox mice were created with exon 1 of the *AR* gene flanked by loxP sites and then were crossed with a knock-in line carrying Cre recombinase under control of the Mlc1f promoter (50). The Mlc1f-Cre transgenic mice were obtained with permission from Steve Burden (Molecular Neurobiology, NYU/New York University School of Medicine, New York, USA). The *AR* gene was located on the X chromosome, and we obtained fmARKO mice at the expected frequencies (Fig. 1*A*). Littermates of AR-flox/Y males and AR-flox-flox females were used as controls in the subsequent experiments. All mice were housed in a specific pathogen-free environment with constant temperature (23 °C ± 1°C), humidity (50% ± 10%), and a 12-h light/dark cycle and with standard feed and clean water. The study protocol was approved by the Animal Care and Use Committee of the University of Tokyo.

Genotyping. The genotypes of the mice were determined by PCR using the following primers: AR FW 5′-AAGTGAATGGTCTTGGC-3′, AR RV 5′-TTACAGGTCTGGTGCAAGCC-3′, Mlc1fCre FW 5′-ACATGTTCAGGGATCGCCAGG-3′, and Mlc1fCre RV 5′-CGCCGCATAACCAGTGAAAC-3′. The AR primers were used to detect the AR-flox allele (430 bp) and the AR wild-type allele (400 bp). The Mlc1fCre primers were used to detect the Mlc1f promoter (250 bp).

Grip Strength Test and Wire Hang Test. Forelimb grip strength was measured by the wire hang test using an MK-380CM/R (Muromachi Kikai) (51). Mice holding a metal grid with their forelimbs were pulled backward by their tails. The gripping force at the point of grip failure was recorded as the grip strength. We measured the grip strength in each mouse in five sequential trials, with 30 s of rest in between (52). All grip strengths were normalized to the mouse's body weight, and the average of three values, excluding the maximum and minimum values, was calculated. The trials were performed for two successive days, and the average of six sets of trials was taken as the representative value for each mouse.

In the forelimb wire hang test, we assessed the ability of mice to exhibit sustained limb tension to oppose gravitational force. Each mouse was placed on top of a wire mesh cage, which was then gently inverted to encourage the mouse to grip the wire; thereafter, the latency to fall (s) was measured. The maximum time to fall among three sequential trials was selected and holding impulse (Ns) was calculated by the following formula: mouse weight (g) × latency to fall (s) × 0.00980665 (gravitational force, N/g) (53, 54).

Treadmill Test. Physical endurance was evaluated using a treadmill for rats and mice (MK-650; Muromachi Kikai). Before evaluation, the mice were made to exercise periodically on the treadmill for 2 d in order for them to adapt to the equipment and electrical stimulation. On the day of evaluation, the mice were kept running on the treadmill at a speed of 10 m/min and an incline of 5%. The treadmill speed was gradually increased by 2 m/min every 5 min (55). When the mice quit running, they were encouraged to run using weak electric stimulation or by gentle tapping or lifting of their hindquarters with a tongue depressor. The cumulative running distance was recorded until the mice were exhausted and continuously touched the shock grids; the power and total work output (J) was calculated by the following formula: mouse weight (g) × vertical travel distance (m) × 0.00980665 (gravitational force, N/g).

Ex Vivo Assessment of the GAST Muscle Contractile Force. Under 2% isoflurane anesthesia, the mouse was kept in prone position, with the temperature maintained at 37 °C. As previously reported, the left GAST muscle was sutured at the distal end and connected to a wide-range force transducer (MLTF500/ST; AD Instruments). Electrical tetanus stimulation (10 V, 50 Hz, 0.1-ms pulse, 5-s duration) was produced by a bipolar platinum electrode, which was placed on the distal cut end of the sciatic nerve, in order to induce a tetanic contractile force in the GAST muscle (56). PowerLab 2/26 Data Acquisition Systems with LabChart V8 (AD Instruments) was used to record and analyze the muscle contractile force.

Tissue Collection, Histology, and Immunofluorescence Staining. For histological and immunohistochemical analyses, muscle tissues and testes were dissected and weighed to an accurate measure of 0.1 mg. The tissues were then fixed with 4% paraformaldehyde for paraffin sections or directly embedded in optimal cutting temperature compound for frozen sections. Transverse sections were cut at 5 μm thickness, followed by H&E, Periodic Acid–Schiff, Oil Red O, NADH-TR, and immunofluorescence staining. Muscle fiber type in the SOL muscles was assessed using mouse monoclonal Anti-Myosin (Skeletal, Fast) antibody (M4276, Thermo Fisher Scientific) and mouse monoclonal Anti-Myosin (Skeletal, Slow) antibody (M8421, Thermo Fisher Scientific), followed by a secondary antibody solution containing Alexa Fluor 488 Goat anti-Mouse IgG (A-11001, Life Technologies). All muscle fibers were examined using BZ-X800 (Keyence), and captured images (10× and 40× views) were quantified using BZ-X800 Analyzer. For quantitative analysis of lipid droplets, we calculated the red pixels in each frame using Photoshop CC software (Adobe Inc.).

Biochemical Assays. Blood samples were collected by cardiac puncture. The serum was separated by centrifugation at 4,500 × g and 4 °C for 10 min and stored at −80 °C until use. The following biochemical parameters were assessed using a 7180 Clinical Analyzer (Hitachi High-Tech Science Co.): testosterone, TC, TG, HDL-C, LDL-C, and adiponectin. Gla-osteocalcin (MK-127, Takara) and TRAP (Immunodiagnostic System) were estimated using enzyme-linked immunosorbent assay (ELISA) kits, following the manufacturer's instructions (57).

Dual-Energy X-ray Absorptiometry (DXA). The BMD of the femur was measured in 13-wk-old mice (n = 3 per group) by DXA using a bone mineral analyzer (DCS-600EX-III R, Aloka). Parameters were measured at 20 points along the long axis, starting from the distal end of the femur, with a 0.75-mm distance between points. Parameters for the trabecular bone were measured at the metaphysis. Parameters for the cortical bone were measured at the midshaft.

Western Blotting. Samples for Western blotting were collected and stored in T-PER (Thermo Fisher Scientific) at −80 °C until use. The samples were homogenized in ice-cold T-PER with Cell Destroyer (Bio Medical Science), and the total protein concentration was determined using BCA protein assays (Thermo Fisher Scientific). Equal amounts of protein (3 to 5 μg of protein sample per well) were loaded on 10% sodium dodecyl sulfate–polyacrylamide electrophoresis gels (SuperSep Ace) and transblotted to polyvinylidene fluoride membranes. The membranes were incubated in blocking buffer (Blocking One, nacalai tesque) for 1 h and then overnight with primary antibodies, including mouse anti-NFATc1 at 1:5,000 dilution (sc-7294, Santa Cruz); rabbit anticalcineurin at 1:5,000 dilution (GTX59619, CST); mouse anti-MyoD at 1:1,000 dilution (sc-377460, Santa Cruz); guinea pig anti-p62/SQSTM1 at 1:5,000 dilution (GP62-C, PROGEN); and mouse antiβ-actin at 1:5,000 dilution (A5441, Sigma-Aldrich). Primary antibodies were detected by incubation with the appropriate secondary antibody for 1 h at room temperature and then with the ECL Prime Western Blotting Substrate (GE Healthcare) for 5 min. Protein expression was measured using WSE-6100LuminoGraph I (ATTO). The densities were measured using ImageJ software (NIH).

Quantitative Real-Time PCR. Total RNA from the GAST muscles was extracted using the RNeasy Fibrous Tissue kit (Qiagen) and reverse transcribed using ReverTra ACE qPCR RT Master Mix (Toyobo). The resulting complementaryDNA was subjected to qPCR analysis using the StepOnePlus™ Real-Time PCR System (Applied Biosystems) with Fast SYBR™ Green Master Mix (Applied Biosystems). Each reaction was run in triplicate using specific primer sets (*SI Appendix,* Table S2). The expression levels of each mRNA were normalized to that of acidic ribosomal phosphoprotein P0 (36B4) and calculated using the comparative critical threshold (Ct) method, as previously described (58).

Microarray Analysis. Total RNA was extracted from the GAST muscles of male control and fmARKO mice (n = 4 per group) and analyzed using Affymetrix mouse genome 430 2.0 array (Thermo Fisher Scientific). Probes with an absolute twofold change and a corrected *P* value of <0.05 were considered significantly different. GO analysis was performed by DNA Chip Research Inc.

LC-MS/MS. The levels of the polyamines PUT, SPD, and SPM in the GAST muscle were measured using the liquid chromatography-tandem mass spectrometry (LC-MS/MS), based on the method previously reported (59). Briefly, 30 to 50 mg of frozen muscle samples were pulverized, extracted in 400 μL MeOH for 1 h, and mixed with the following isotopically labeled internal standards: putrescine-d8 (D416027, Toronto Research Chemicals); SPD-d6 (D367002, Toronto Research Chemicals); and SPM-d20 (S680512, Toronto Research Chemicals). For the removal of lipids, we followed the Folch's extraction procedure (60). Specifically, we added 800 μL chloroform and 200 μL water to the mixture, which was centrifuged at 15,000 rpm for 3 min before transferring the upper phase to a new tube for evaporation. Samples were resuspended in 150 μL of 0.2 M carbonate-bicarbonate buffer (pH 9), 180 μL of acetone, and 120 μL of 10 mg/mL dansyl chloride (Wako), and incubated at 37° for 1 h. Then, 50 μL of 100 mg/mL proline in water was added to quench the unreacted dansyl chloride and incubated for 10 min. Then, derivatized samples were purified by liquid–liquid extraction with 500 μL of ethyl acetate. LC-MS/MS analysis was performed using an LCMS-8060 triple quadrupole mass spectrometer (Shimadzu Co.). The reversed-phase chromatographic separation was performed on a Kinetex EVO C18 analytical column (2.6 μm, 2.1 mm × 150 mm) (Phenomenex) as previously reported (59).

Primary Culture of Myoblasts and Evaluation of Polyamine Levels. Myoblasts were isolated from muscles and cultured on collagen-coated dishes at 37 °C with 5% CO_2 until confluence (61, 62). The growth medium comprised Ham's F-10 Nutrient Mix, 20% fetal bovine serum, 100 units/mL of penicillin, 100 μg/mL of streptomycin, and 2 ng/mL of basic fibroblast growth factor. We treated the myotubes with vehicle alone or 100 nM of DHT, which is the most biologically active form of endogenous androgen, for 24 h. Thereafter, the cells were protected from light and incubated for 30 min at 37 °C with 20 μM PolyamineRED (Funakoshi) and 8.1 μM Hoechst33342 (Thermo Fisher Scientific) (63). The polyamine levels were evaluated by fluorescence microscopy, and the red pixels in each frame were calculated using Photoshop CC software (Adobe Inc.).

Statistical Analyses. All data were presented as mean ± SE of the mean. Unless otherwise specified, unpaired Student's *t* test was performed to evaluate the differences between fmARKO and control mice. One-way ANOVA with the post hoc Tukey test was used to determine the statistical significance for multigroup comparisons. The significance level was set at a *P* value of <0.05. All statistical analyses were performed with Microsoft Excel (Microsoft Corp.) and GraphPad Prism 9 (GraphPad Software), except the GO analysis, which was performed using the GeneSpring ver. 14.9.1 (Agilent Technologies).

Data, Materials, and Software Availability. All study data are included in the article and/or *SI Appendix*.

ACKNOWLEDGMENTS. We thank K. Shigemoto and N. Motohashi of Tokyo Metropolitan Institute of Gerontology for their generous help and instruction and for teaching us the skills required to perform myoblast primary culture experiments for molecular analysis. This work was supported by a Grant-in-Aid for Scientific Research from the Japan Society for the Promotion of Science (JSPS KAKENHI Grant Numbers 18K07463 and 22K07465), AMED under Grant Number JP22dk0110047, and a grant by Okinaka Memorial Institute for Medical Research.

Author affiliations: [a]Department of Geriatric Medicine, Graduate School of Medicine, The University of Tokyo, Bunkyo-ku, Tokyo 113-0033, Japan; [b]Department of Diabetes and Metabolic Diseases, Graduate School of Medicine, The University of Tokyo, Bunkyo-ku, Tokyo 113-0033, Japan; [c]Diabetes Research Center, National Center for Global Health and Medicine, Shinjuku-ku, Tokyo 162-8655, Japan; [d]Fukushima Medical University, Fukushima 960-1295, Japan; [e]Department of Lipidomics, Graduate School of Medicine, The University of Tokyo, 7-3-1 Hongo, Bunkyo-ku, Tokyo 113-0033, Japan; [f]Department of Hematology, Endocrinology and Metabolism, Tokushima University Graduate School, Tokushima 770-8503, Japan; and [g]Fujii Memorial Institute of Medical Sciences, Institute of Advanced Medical Sciences, Tokushima University, Tokushima 770-8503, Japan

1. M. Yakabe, T. Hosoi, M. Akishita, S. Ogawa, Updated concept of sarcopenia based on muscle-bone relationship. *J. Bone Miner. Metab.* **38**, 7–13 (2019).
2. A. J. Cruz-Jentoft, A. A. Sayer, Sarcopenia. *Lancet* **393**, 2636–2646 (2019).
3. T. Lang *et al.*, Sarcopenia: Etiology, clinical consequences, intervention, and assessment. *Osteoporos. Int.* **21**, 543–559 (2010).
4. J. Talbot, L. Maves, Skeletal muscle fiber type: Using insights from muscle developmental biology to dissect targets for susceptibility and resistance to muscle disease. *Wiley Interdiscip. Rev. Dev. Biol.* **5**, 518–534 (2016).
5. D. A. Monks, M. M. Holmes, Androgen receptors and muscle: A key mechanism underlying life history trade-offs. *J. Comp. Physiol. A Neuroethol. Sens. Neural. Behav. Physiol.* **204**, 51–60 (2018).
6. S. E. Borst, Interventions for sarcopenia and muscle weakness in older people. *Age Ageing* **33**, 548–555 (2004).
7. M. D. O'Connell, F. C. Wu, Androgen effects on skeletal muscle: Implications for the development and management of frailty. *Asian J. Androl.* **16**, 203–212 (2014).
8. K. J. Ottenbacher, M. E. Ottenbacher, A. J. Ottenbacher, A. A. Acha, G. V. Ostir, Androgen treatment and muscle strength in elderly males: A meta-analysis. *J. Am. Geriatr. Soc.* **54**, 1666–1673 (2006).
9. M. H. Emmelot-Vonk *et al.*, Effect of testosterone supplementation on functional mobility, cognition, and other parameters in older men: A randomized controlled trial. *JAMA* **299**, 39–52 (2008).
10. F. Claessens *et al.*, Diverse roles of androgen receptor (AR) domains in AR-mediated signaling. *Nucl. Recept Signal* **6**, e008 (2008).
11. T. Matsumoto *et al.*, The androgen receptor in health and disease. *Annu. Rev. Physiol.* **75**, 201–224 (2013).
12. V. Dubois, M. Laurent, S. Boonen, D. Vanderschueren, F. Claessens, Androgens and skeletal muscle: Cellular and molecular action mechanisms underlying the anabolic actions. *Cell Mol. Life Sci.* **69**, 1651–1667 (2012).
13. K. De Gendt, G. Verhoeven, Tissue- and cell-specific functions of the androgen receptor revealed through conditional knockout models in mice. *Mol. Cell Endocrinol.* **352**, 13–25 (2012).
14. H. E. MacLean *et al.*, Impaired skeletal muscle development and function in male, but not female, genomic androgen receptor knockout mice. *FASEB J.* **22**, 2676–2689 (2008).
15. J. Ophoff *et al.*, Androgen signaling in myocytes contributes to the maintenance of muscle mass and fiber type regulation but not to muscle strength or fatigue. *Endocrinology* **150**, 3558–3566 (2009).
16. C. Chambon *et al.*, Myocytic androgen receptor controls the strength but not the mass of limb muscles. *Proc. Natl. Acad. Sci. U.S.A.* **107**, 14327–14332 (2010).
17. S. Schiaffino, C. Reggiani, Myosin isoforms in mammalian skeletal muscle. *J. Appl. Physiol.* **77**, 493–501 (1994).
18. W. M. Gerald *et al.*, Selective expression of Cre recombinase in skeletal muscle fibers. *Genesis* **26**, 165–166 (2002).
19. V. Augusto, C. R. Padovani, G. E. R. Campos, Skeletal muscle fiber types in C57BL6J mice. *Braz. J. Morphol. Sci.* **21**, 89–94 (2004).
20. F. Oury *et al.*, Endocrine regulation of male fertility by the skeleton. *Cell* **144**, 796–809 (2011).
21. P. Wagner, R. Chapurlat, R. Ecochard, P. Szulc, Low muscle strength and mass is associated with the accelerated decline of bone microarchitecture at the distal radius in older men: The prospective STRAMBO study. *J. Bone Miner. Res.* **33**, 1630–1640 (2018).
22. E. Manieri *et al.*, Adiponectin accounts for gender differences in hepatocellular carcinoma incidence. *J. Exp. Med.* **216**, 1108–1119 (2019).
23. J. Francisco *et al.*, Stimulation of slow skeletal muscle fiber gene expression by calcineurin in vivo. *J. Biol. Chem.* **275**, 4545–4548 (2000).
24. J. Du *et al.*, The regulation of skeletal muscle fiber-type composition by betaine is associated with NFATc1/MyoD. *J. Mol. Med. (Berl.)* **96**, 685–700 (2018).
25. R. Macharia, A. Otto, P. Valasek, K. Patel, Neuromuscular junction morphology, fiber-type proportions, and satellite-cell proliferation rates are altered in MyoD(-/-) mice. *Muscle Nerve* **42**, 38–52 (2010).
26. V. Dubois *et al.*, A satellite cell-specific knockout of the androgen receptor reveals myostatin as a direct androgen target in skeletal muscle. *FASEB J.* **28**, 2979–2994 (2014).
27. L. A. Tintignac *et al.*, Degradation of MyoD mediated by the SCF (MAFbx) ubiquitin ligase. *J. Biol. Chem.* **280**, 2847–2856 (2005).
28. J. Lagirand-Cantaloube *et al.*, Inhibition of atrogin-1/MAFbx mediated MyoD proteolysis prevents skeletal muscle atrophy in vivo. *PLoS One* **4**, e4973 (2009).
29. K. Rana, N. K. Lee, J. D. Zajac, H. E. MacLean, Expression of androgen receptor target genes in skeletal muscle. *Asian J. Androl.* **16**, 675–683 (2014).
30. E. R. Chin *et al.*, A calcineurin-dependent transcriptional pathway controls skeletal muscle fiber type. *Genes Dev.* **12**, 2499–2509 (1998).
31. N. K. Lee, J. P. Skinner, J. D. Zajac, H. E. MacLean, Ornithine decarboxylase is upregulated by the androgen receptor in skeletal muscle and regulates myoblast proliferation. *Am. J. Physiol. Endocrinol. Metab.* **301**, E172–179 (2011).
32. N. K. Lee, H. E. MacLean, Polyamines, androgens, and skeletal muscle hypertrophy. *J. Cell Physiol.* **226**, 1453–1460 (2011).
33. R. Uchitomi *et al.*, Metabolomic analysis of skeletal muscle in aged mice. *Sci. Rep.* **9**, 10425 (2019).
34. D. U. Kemaladewi, J. S. Benjamin, E. Hyatt, E. A. Ivakine, R. D. Cohn, Increased polyamines as protective disease modifiers in congenital muscular dystrophy. *Hum. Mol. Genet.* **27**, 1905–1912 (2018).
35. T. Eisenberg *et al.*, Induction of autophagy by spermidine promotes longevity. *Nat. Cell Biol.* **11**, 1305–1314 (2009).
36. M. Cervelli *et al.*, Skeletal muscle pathophysiology: The emerging role of spermine oxidase and spermidine. *Med. Sci. (Basel)* **6**, 14 (2018).
37. E. Masiero *et al.*, Autophagy is required to maintain muscle mass. *Cell Metab.* **10**, 507–515 (2009).
38. L. Garcia-Prat *et al.*, Autophagy maintains stemness by preventing senescence. *Nature* **529**, 37–42 (2016).
39. Y. Kitajima *et al.*, Proteasome dysfunction induces muscle growth defects and protein aggregation. *J. Cell Sci.* **127**, 5204–5217 (2014).
40. M. L. Ehlers, B. Celona, B. L. Black, NFATc1 controls skeletal muscle fiber type and is a negative regulator of MyoD activity. *Cell Rep.* **8**, 1639–1648 (2014).
41. D. J. Seward, J. C. Haney, M. A. Rudnicki, S. J. Swoap, bHLH transcription factor MyoD affects myosin heavy chain expression pattern in a muscle-specific fashion. *Am. J. Physiol. Cell Physiol.* **280**, C408–C413 (2001).
42. Y. Kanno *et al.*, Selective androgen receptor modulator, YK11, regulates myogenic differentiation of C2C12 myoblasts by follistatin expression. *Biol. Pharm. Bull.* **36**, 1460–1465 (2013).
43. T. Yamamoto *et al.*, The natural polyamines spermidine and spermine prevent bone loss through preferential disruption of osteoclastic activation in ovariectomized mice. *Br. J. Pharmacol.* **166**, 1084–1096 (2012).
44. J. D. Méndez, R. D. H. Hernández, L-arginine and polyamine administration protect beta-cells against alloxan diabetogenic effect in Sprague-Dawley rats. *Biomed. Pharmacother.* **59**, 283–289 (2005).
45. M. Al-Habsi *et al.*, Spermidine activates mitochondrial trifunctional protein and improves antitumor immunity in mice. *Science* **378**, eabj3510 (2022).
46. J. Jell *et al.*, Genetically altered expression of spermidine/spermine N1-acetyltransferase affects fat metabolism in mice via acetyl-CoA. *J. Biol. Chem.* **282**, 8404–8413 (2007).
47. K. Soda *et al.*, Long-term oral polyamine intake increases blood polyamine concentrations. *J. Nutr. Sci. Vitaminol. (Tokyo)* **55**, 361–366 (2009).
48. R. Katagiri *et al.*, Association of soy and fermented soy product intake with total and cause specific mortality: Prospective cohort study. *BMJ* **368**, m34 (2020).
49. J. Fan *et al.*, Autophagy as a potential target for sarcopenia. *J. Cell Physiol.* **231**, 1450–1459 (2016).
50. S. Yeh *et al.*, Generation and characterization of androgen receptor knockout (ARKO) mice: An in vivo model for the study of androgen functions in selective tissues. *Proc. Natl. Acad. Sci. U.S.A.* **99**, 13498–13503 (2002).
51. O. A. Meyer, H. A. Tilson, W. C. Byrd, M. T. Riley, A method for the routine assessment of fore- and hindlimb grip strength of rats and mice. *Neurobehav. Toxicol.* **3**, 233–236 (1979).
52. L. Y. Juo *et al.*, HSPB7 interacts with dimerized FLNC and its absence results in progressive myopathy in skeletal muscles. *J. Cell Sci.* **129**, 1661–1670 (2016).
53. R. Fan *et al.*, Beneficial effects of walnut oligopeptides on muscle loss in senescence-accelerated mouse prone-8 (SAMP8) mice: Focusing on mitochondrial function. *Nutrients* **14**, 2051 (2022).
54. A. Huizer-Pajkos *et al.*, Adverse geriatric outcomes secondary to polypharmacy in a mouse model: The influence of aging. *J. Gerontol. A Biol. Sci. Med. Sci.* **71**, 571–577 (2016).
55. C. Canto *et al.*, AMPK regulates energy expenditure by modulating NAD+ metabolism and SIRT1 activity. *Nature* **458**, 1056–1060 (2009).
56. R. M. Corrick *et al.*, Dexamethasone protects against tourniquet-induced acute ischemia-reperfusion injury in mouse hindlimb. *Front. Physiol.* **9**, 244 (2018).
57. K. Steinfeld *et al.*, Low testosterone in ApoE/LDL receptor double-knockout mice is associated with rarefied testicular capillaries together with fewer and smaller Leydig cells. *Sci. Rep.* **8**, 5424 (2018).
58. K. J. Livak, T. D. Schmittgen, Analysis of relative gene expression data using real-time quantitative PCR and the 2(-delta delta C(T)) method. *Methods* **25**, 402–408 (2001).
59. I. Samarra *et al.*, Gender-related differences on polyamine metabolome in liquid biopsies by a simple and sensitive two-step liquid-liquid extraction and LC-MS/MS. *Biomolecules* **9**, 779 (2019).
60. L. F. Eggers, D. Schwudke, "Liquid extraction: Folch" in *Encyclopedia of Lipidomics*, M. Wenk, Ed. (Springer, Dordrecht, 2016).
61. N. Motohashi, Y. Asakura, A. Asakura, Isolation, culture, and transplantation of muscle satellite cells. *J. Vis. Exp.* **8**, 50486 (2014).
62. T. Takaya, Y. Nihashi, S. Kojima, T. Ono, H. Kagami, Autonomous xenogenic cell fusion of murine and chick skeletal muscle myoblasts. *Animal Sci. J.* **88**, 1880–1885 (2017).
63. K. K. H. Vong *et al.*, Cancer cell targeting driven by selective polyamine reactivity with glycine propargyl esters. *Chem. Commun. (Camb.)* **53**, 8403–8406 (2017).